ISSN 1001-0742
CN 11-2629/X

JES

JOURNAL OF ENVIRONMENTAL SCIENCES

March 1, 2015 Volume 29
www.jesc.ac.cn

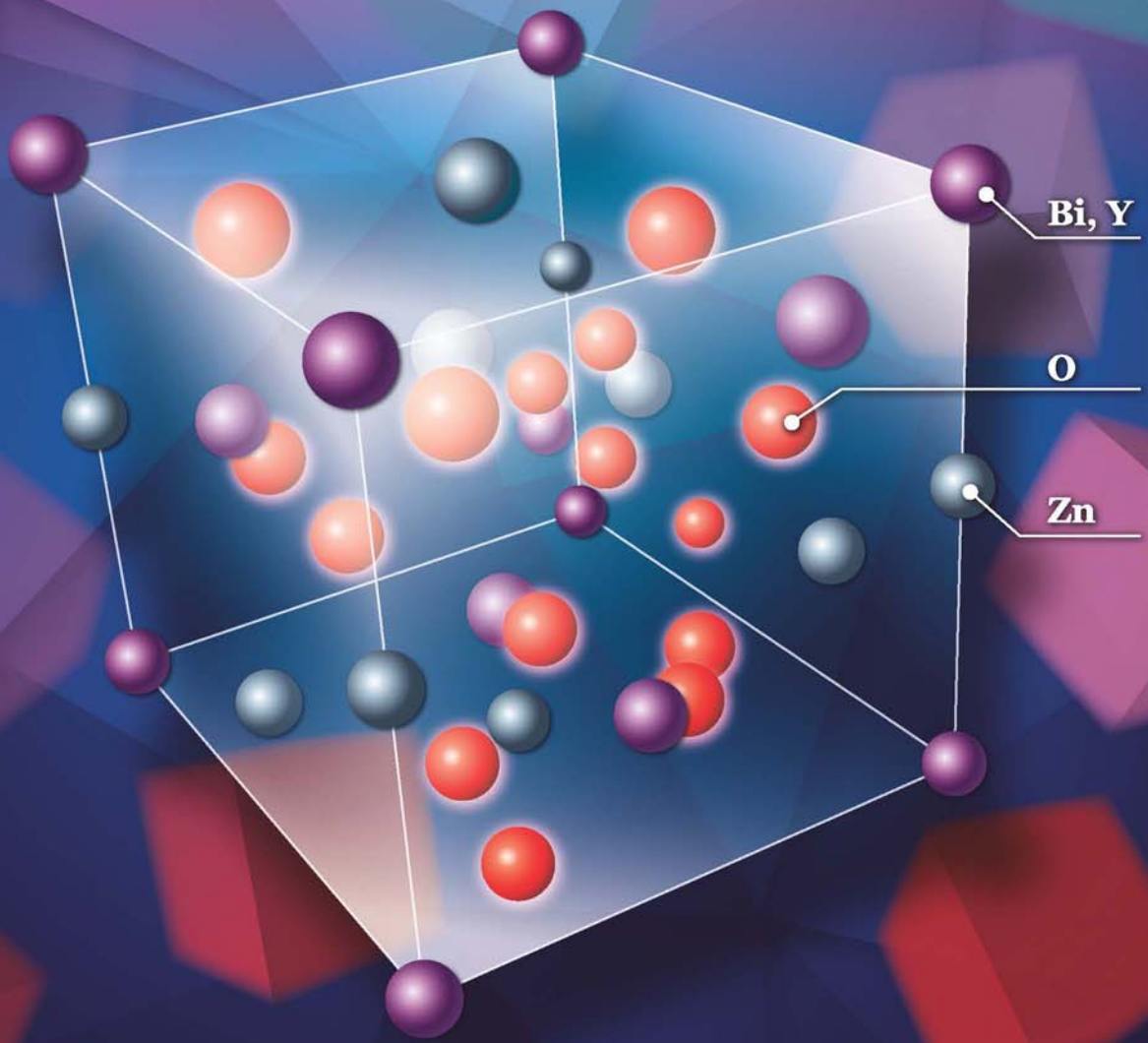

ELSEVIER
Science Press

Sponsored by
Research Center for Eco-Environmental Sciences
Chinese Academy of Sciences

Journal of Environmental Sciences Volume 29 2015

www.jesc.ac.cn

(continued on inside back cover)

CONTENTS

Available online at www.sciencedirect.com

ScienceDirect

www.journals.elsevier.com/journal-of-environmental-sciences

JOURNAL OF ENVIRONMENTAL SCIENCES
www.jesc.ac.cn

Flower-, wire-, and sheet-like MnO_2-deposited diatomites: Highly efficient absorbents for the removal of Cr(VI)

Yucheng Du[1,*], *Liping Wang*[1], *Jinshu Wang*[1,*], *Guangwei Zheng*[1], *Junshu Wu*[1], *Hongxing Dai*[2,*]

1. *Key Lab of Advanced Functional Materials, Ministry of Education, College of Materials Science and Engineering, Beijing University of Technology, Beijing 100124, China. E-mail: ychengdu@bjut.edu.cn*
2. *Laboratory of Catalysis Chemistry and Nanoscience, Department of Chemistry and Chemical Engineering, College of Environmental and Energy Engineering, Beijing University of Technology, Beijing 100124, China*

ARTICLE INFO

Article history:
Received 3 April 2014
Revised 4 June 2014
Accepted 13 June 2014
Available online 23 December 2014

Keywords:
Morphological effect
MnO_2-deposited diatomite
Cr(VI) removal
Adsorption efficiency

ABSTRACT

Flower-, wire-, and sheet-like MnO_2-deposited diatomites have been prepared using a hydrothermal method with $Mn(Ac)_2$, $KMnO_4$ and/or $MnSO_4$ as Mn source and diatomite as support. Physical properties of the materials were characterized by means of numerous analytical techniques, and their behaviors in the adsorption of chromium(VI) were evaluated. It is shown that the MnO_2-deposited diatomite samples with different morphologies possessed high surface areas and abundant surface hydroxyl groups (especially the wire-like MnO_2/diatomite sample). The wire-like MnO_2/diatomite sample showed the best performance in the removal of Cr(VI), giving the maximum Cr(VI) adsorption capacity of 101 mg/g.

Introduction

Cr(VI) and Cr(III) ions are toxic and can lead to mutagenicity and potential carcinogenicity due to their long-time retention in the human body (Gülay and Mehmet, 2008). The pollutants are emitted from the industrial activities of electroplating, pigments, metal cleaning, leather processing, and mining (Metin et al., 2008). It is well known that toxic chromium mainly exists in two oxidation states (*i.e.*, Cr(VI) or Cr(III)) (Martell and Hancock, 1996), of which the hexavalent chromium shows a much higher toxicity than the trivalent chromium because of the stable valence of the former (Farag et al., 2006). Cr(VI) is carcinogenic and mutagenic for living organisms, easily absorbed by the human body, and accumulated in the body (Pagana et al., 2011). Therefore, it is highly desirable to treat Cr(VI)-containing wastewater.

Up to now, numerous methods such as precipitation (Almeida and Boaventura, 1997), ion exchange (Gzara and Dhahbi, 2001), membrane separation (Kozlowski and Walkowiak, 2002), reduction (Williford et al., 2002), biosorption (Mohanty et al., 2006), and adsorption (Mohanty et al., 2005) have been utilized to remove Cr(VI) from wastewater. Among these methods, adsorption (especially chemisorption) is considered to be particularly feasible and effective (Muradiye and Irfan, 2007). In the past years, a number of works have been focused on the removal of Cr(VI) with adsorbents such as surfactant-modified activated carbon (Choi et al., 2009), macroporous polystyrene (Cui et al., 2013), tamarind seeds (Gupta and Babu, 2009), and acetate/silica composite nanofibers (Taha et al., 2012). However, these adsorbents are not effective for the removal of Cr(VI). Hence, an alternative and low-cost adsorbent needs to be developed to purify Cr(VI)-containing wastewater.

* *Corresponding authors.* E-mails: ychengdu@bjut.edu.cn (Yucheng Du), wangjsh@bjut.edu.cn (Jinshu Wang), hxdai@bjut.edu.cn (Hongxing Dai).

http://dx.doi.org/10.1016/j.jes.2014.06.047
1001-0742/

Diatomite-based materials are abundant from natural sources, large in surface area, stable in chemical properties, and good in adsorption ability (Al-Ghouti and Al-Degs, 2011). In recent years, Al-Degs et al. (2001), Khraisheh et al. (2004), Al-Ghouti et al. (2004), and Li et al. (2009) prepared manganese oxide-loaded diatomite adsorbents, and observed that these materials showed good adsorption capacities for the removal of Pb(II), Cu(II), Cd(II), Zn(II), and Cr(III). Diatomite, however, does not exhibit effective adsorption for the negatively charged heavy metal oxide ions (*e.g.*, $HCrO_4^-$, CrO_4^{2-}, $Cr_2O_7^{2-}$, $H_2AsO_3^-$, $HAsO_3^{2-}$, AsO_3^{3-}, $H_2AsO_4^-$, $HAsO_4^{2-}$, and AsO_4^{3-}) in water, and gave a Cr(VI) removal efficiency of only 65% (Sungworawongpana and Pengprecha, 2011). Hence, it is necessary to modify diatomite so that its adsorption capacity of negatively charged heavy metal oxides can be enhanced substantially. In a review article, Danil de Namor et al. (2012) summarized the extraction results of heavy metals from water using diatomite and modified diatomite samples, in which most of the modified diatomites were composed of mechanical mixtures of diatomite and modifiers (*e.g.*, salts of iron, manganese, and aluminum, and organic matter).

To the best of our knowledge, the use of ordered nanostructural metal oxide-modified diatomites for the removal of heavy metal ions from water has been rarely reported. In this study, we prepared diatomite-supported MnO_2 with various morphologies, and examined the behavior in Cr(VI) adsorption. It was found that the MnO_2-deposited diatomite materials possessed excellent Cr(VI) adsorption performance.

1. Experimental

1.1. Preparation of MnO_2-deposited diatomites with different morphologies

Industrial-grade diatomite (Jilin Changbai, China) was used as received without further purification. Analytical grade manganese sulfate monohydrate ($MnSO_4{\cdot}H_2O$), manganese acetate tetrahydrate ($Mn(Ac)_2{\cdot}4H_2O$), potassium permanganate ($KMnO_4$), potassium hydroxide (KOH), and ammonium persulfate ($(NH_4)_2S_2O_8$) were purchased from Beijing Chemical Reagent Company.

The MnO_2-coated diatomite samples with different morphologies were prepared using a hydrothermal method. The detailed procedures are as follows: (1) 2.7918 g of $Mn(Ac)_2$ was dissolved in 20 mL of deionized water, and the desired amount ($Mn(Ac)_2/KMnO_4$ molar ratio = 3:2) of $KMnO_4$ was dissolved in 20 mL of deionized water. The $Mn(Ac)_2$ aqueous solution was added dropwise to a suspension of diatomite (0.1 g/mL) and stirred in a thermostatted vessel for 0.5 hr. Then, the $KMnO_4$ aqueous solution was added to the above mixed solution. After being stirred for 0.5 hr, the mixture was transferred into a Teflon-lined stainless steel autoclave (100 mL) for hydrothermal treatment at 80°C for 4 hr. The wet solid was filtered, washed with deionized water three times, and dried at 60°C for 10 hr, thus obtaining the flower-like MnO_2/diatomite sample. (2) 2.212 g of $KMnO_4$ was dissolved in 20 mL of deionized water, and a desired amount ($KMnO_4/(NH_4)_2S_2O_8$ molar ratio = 1:1) of $(NH_4)_2S_2O_8$ was dissolved in 20 mL of deionized water. The $KMnO_4$ aqueous solution was added dropwise to a suspension of diatomite (0.1 g/mL) and stirred in a thermostatted vessel for 0.5 hr. Then, the $(NH_4)_2S_2O_8$ aqueous solution was added to the above mixed solution. After being stirred for 0.5 hr, the mixture was transferred into a Teflon-lined stainless steel autoclave (100 mL) for hydrothermal treatment at 90°C for 12 hr. The wet solid was filtered, washed with deionized water three times, and dried at 60°C for 8 hr, thus obtaining the wire-like MnO_2/diatomite sample. (3) A $MnSO_4$ aqueous solution (0.2 mol/L) was added dropwise to a suspension of diatomite (0.1 g/mL) and stirred in a thermostatted vessel for 0.5 hr. Then, the desired amounts ($MnSO_4/(NH_4)_2S_2O_8$ molar ratio = 1:1) of $(NH_4)_2S_2O_8$ and KOH aqueous solution (1.2 mol/L) were added to the above mixed solution. After being stirred for 0.5 hr, the mixture was transferred into a Teflon-lined stainless steel autoclave (100 mL) for hydrothermal treatment at room temperature for 12 hr. The wet solid was filtered, washed with deionized water three times, and dried at 100°C for 8 hr, thus obtaining the sheet-like MnO_2/diatomite sample.

1.2. Sample characterization

X-ray diffraction (XRD) patterns of the samples in the 2θ range of 10°–80° were determined on a D/MAX-II X-ray diffractometer with Cu $K\alpha$ radiation and nickel filter (λ = 0.15406 nm). The instrument was operated at 35 mA and 35 kV with a scanning speed of 4°/min and a step size of 0.02°. The crystal phases of the samples were identified by referring to the JCPDS Database. The scanning electron microscopic (SEM) images of the samples were recorded on a Hitachi 570 instrument. The transmission electron microscopic (TEM) and high-resolution (HRTEM) images of the samples were obtained on a Hitachi H-9000 NAR apparatus (operating voltage = 250 kV). The specific surface areas and pore-size distributions of the samples were measured using nitrogen adsorption at −196°C on an ASAP 2020 apparatus. The elemental compositions of the samples were determined using inductively coupled plasma atomic emission spectroscopy (ICP-AES). Fourier transform infrared (FT-IR) spectra of the samples (1 wt.% sample + 99 wt.% KBr) were obtained in the range of 400–4000 cm^{-1} with a resolution of 0.4 cm^{-1} on a Perkin-Elmer 1730 spectrometer. X-ray photoelectron spectroscopy (Ulvac-PHI, PHI Quantera) was employed to determine the O 1s and C 1s binding energies of the samples using Al $K\alpha$ ($h\upsilon$ = 1486.7 eV) as excitation source, and the C 1s signal at 284.6 eV was used to calibrate the binding energies.

1.3. Cr(VI) adsorption

Cr(VI) aqueous 50 or 100 mL solution with a concentration of 10, 25, 50, 75, 100, 125, 150, 175, 200, 225 or 250 mg/L was placed in a conical flask, which was prepared using $K_2Cr_2O_7$ as Cr source. The pH value of the Cr(VI)-containing solution was adjusted to 1,2, 3, 4, 6, 7, 8, 9 or 10 using aqueous solutions of HCl (2 mol/L) or NaOH (2 mol/L). 0.04 g of the MnO_2/diatomite was added to the Cr(VI) solution, followed by oscillation for 10 min, 0.5, 1, 1.5, 2, 3, 4 or 5 hr at room temperature. After that, the mixed solution was centrifuged and the Cr(VI) concentration was detected using a UV spectrophotometer (SP-750, Shanghai).

In the adsorption experiment, 40 mg of the sample was put into 100 mL of the Cr(VI) aqueous solution (250 mg/L) under magnetic stirring. After Cr(VI) adsorption for 4 hr, the sample solution was allowed to settle. The Cr(VI) concentration in the

supernatant was analyzed using the ICP-AES technique, and the maximal Cr(VI) adsorption capacity of the sample was calculated according to Eq. (2) below. In the desorption experiment, the Cr(VI)-adsorbed sample solution was filtered and the solid was put into 100 mL of H_2SO_4 aqueous solution (20 wt.%) under stirring for 2 hr. After Cr(VI) desorption, the sample solution was filtered again. The desorption operation was repeated twice. The Cr(VI) adsorption/desorption recycling was conducted 8 times.

The Cr(VI) removal efficiency and equilibrium Cr(VI) adsorption capacity were calculated according to Eqs. (1) and (2), respectively.

$$E(\%) = \frac{C_0 - C_e}{C_0} \times 100\% \quad (1)$$

$$Q_e = \frac{(C_0 - C_e)\ V}{m} \quad (2)$$

where, E, Q_e, C_0, C_e, V, and m are the Cr(VI) removal efficiency, equilibrium Cr(VI) adsorption capacity (mg/g), initial Cr(VI) concentration (mg/L), equilibrium Cr(VI) concentration (mg/L), solution volume (L), and adsorbent mass (g), respectively.

2. Results and discussion

2.1. Crystal phase composition

Fig. 1 shows the XRD patterns of the samples. It can be observed that the XRD pattern of the diatomite sample showed a broad peak at 2θ = 22.6° (Fig. 1a), assignable to amorphous SiO_2; the diffraction peaks corresponding to the (100) and (101) crystal planes were due to quartz impurities. After loading of MnO_2 (Fig. 1b, c, and d), the diffraction signal of diatomite was still retained, suggesting that the amorphous SiO_2 structure in diatomite was not changed. Due to the different configurations of the [MnO_6] octahedral unit, MnO_2 can show various polymorphs (Julien and Massot, 2002). The flower-like MnO_2/diatomite sample showed three broad peaks

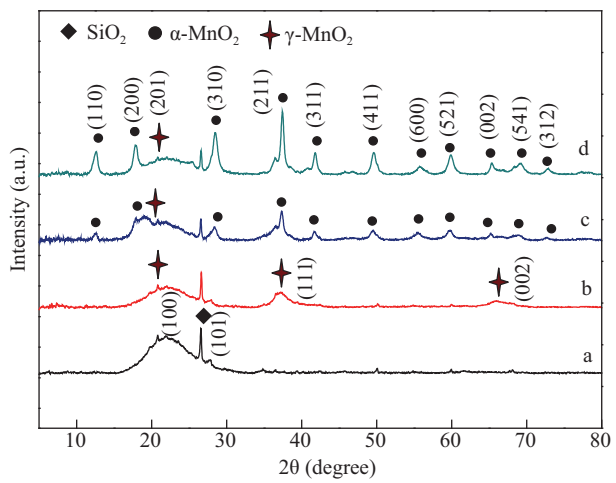

Fig. 1 – XRD patterns of (line a) diatomite, (line b) flower-like MnO_2/diatomite, (line c) wire-like MnO_2/diatomite, and (line d) sheet-like MnO_2/diatomite.

at 2θ = 21.9°, 37.2°, and 67.3° (Fig. 1b), which could be indexed to birnessite-type γ-MnO_2 (JCPDS PDF# 14-0644), similar to the γ-MnO_2 crystallites (Yuan et al., 2010a,b). Compared to the flower-like MnO_2/diatomite sample, the other MnO_2/diatomite samples contained mixed MnO_2 crystal phases (Fig. 1c and d): birnessite-type γ-MnO_2 in minority and tetragonal α-MnO_2 in majority. The lattice parameters of the latter phase were: $a = b = 0.9784 \pm 0.0014$ nm and $c = 0.2846 \pm 0.0008$ nm, in good agreement with the reported data ($a = b = 0.9782$ nm and $c = 0.2853$ nm) of the standard α-MnO_2 sample (JCPDS PDF# 44-0140). The strong and sharp diffraction peaks indicate the formation of MnO_2 nanoparticles with good crystallinity.

2.2. Morphology, pore structure, and surface area

The different shapes of MnO_2 were generated due to the use of different preparation conditions (manganese sources, reactants, reaction temperature and reaction time). The morphologies of the samples are shown in Fig. 2. The diatomite sample possessed a disk-like morphology with a uniform ordered porous structure, with the diameter of each disk about 25 μm. There were a large number of flower-, wire-, and sheet-like MnO_2 nanoparticles randomly deposited on the surface of the diatomite. The TEM and high-resolution TEM images further confirm the morphologies of the MnO_2-coated diatomite samples. Well-grown flower-, wire-, and sheet-like MnO_2 nanoparticles and diatomite were observed. From the high-resolution TEM images (Fig. 3c, f, i, and l), one can see that (i) the lattice spacings (d values) of the (111) and (201) crystal planes of the flower-like MnO_2/diatomite sample were 0.230 and 0.408 nm, respectively, rather close to those (0.23437 and 0.40722 nm) of the standard γ-MnO_2 sample (JCPDS PDF# 14-0644); (ii) the d values (0.242 and 0.310 nm) of the (211) and (310) crystal planes of the wire-like MnO_2/diatomite sample were in good accordance with those of the standard α-MnO_2 sample (JCPDS PDF# 44-0140); and (iii) the d value (0.490 nm) of the (200) crystal plane of the sheet-like MnO_2/diatomite sample was also not far away from that (0.48950 nm) of the standard α-MnO_2 sample (JCPDS PDF# 44-0140). Furthermore, the recording of multiple bright electron diffraction rings in the SAED patterns (insets of Fig. 3c, f, and i) indicates that the MnO_2-coated diatomite samples were polycrystalline.

Diatomite shows a mesh-like structure with a network of bridging silicon-oxygen tetrahedra. Due to the uncertainty of the number of silicon atoms, coordination defects and oxygen bridge defects exist in the mesh-like structure (Sheng et al., 2009). Hence, it is easy to form surface silanols (Si–OH) due to the combination of H with the surface Si–O dangling bonds. Dissociation of surface silanols usually occurs in water into $Si–O^-$ and H^+, making the surface of diatomite negatively charged (Zhuravlev, 2000).

Fig. 4 shows the N_2 adsorption–desorption isotherms and pore-size distributions of the samples. The flower-, wire-, and sheet-like MnO_2/diatomite samples showed a type II isotherm with a hysteresis loop resembling H3 and H4 types, indicating the presence of porous structures (Yuan et al., 2010a,b). The pore-size distributions of the samples confirm the presence of meso- and macropores. As shown in Table 1, the BET surface areas of the flower-, wire-, and sheet-like MnO_2/diatomite

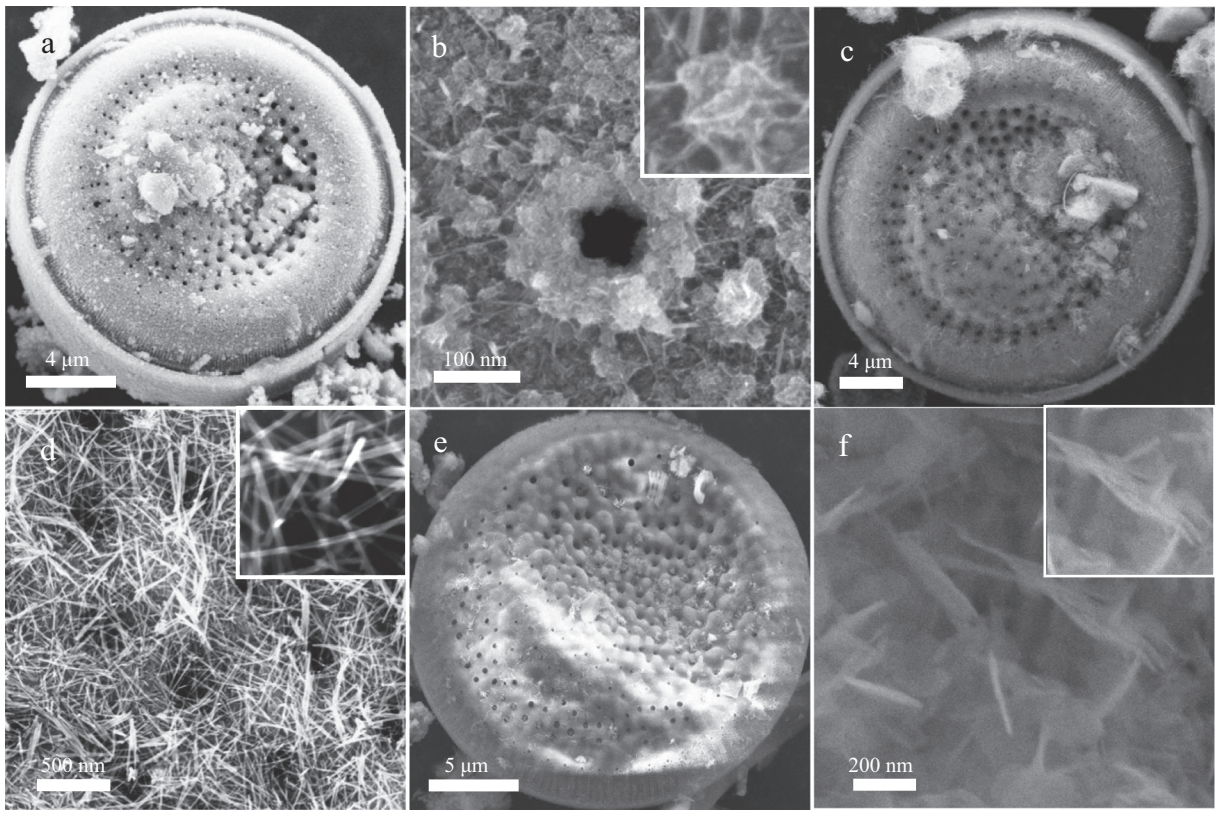

Fig. 2 – SEM images of (a, b) flower-like MnO_2/diatomite, (c, d) wire-like MnO_2/diatomite, and (e, f) sheet-like MnO_2/diatomite.

samples were 66.5, 144.2, and 49.5 m^2/g, respectively, much higher than that (25 m^2/g) of the diatomite sample.

2.3. Cr(VI) adsorption property

2.3.1. Influence of pH on the adsorption of Cr(VI)

Fig. 5 shows the effect of pH value on the Cr(VI) removal efficiency of the diatomite and MnO_2/diatomite samples under the conditions of Cr(VI) solution volume = 100 mL, initial Cr(VI) concentration = 50 mg/L, adsorbent mass = 0.04 g, adsorption time = 30 min, and adsorption temperature = room temperature. It was observed that the maximal Cr(VI) removal efficiency reached 99.98% at pH = 2 or 8. Cr(VI) species in solution could be present in the form of dichromate ($Cr_2O_7^{2-}$), hydrochromate ($HCrO_4^-$) or chromate (CrO_4^{2-}). In an acidic environment (lower pH values), Cr(VI) exists in $HCrO_4^-$ or $Cr_2O_7^{2-}$, whereas in an alkaline environment (higher pH values), it exists predominately in CrO_4^{2-} (Ajouyed et al., 2010; Han et al., 2008; Ajmal et al., 1996). When pH < 2, the surface of MnO_2 became more positively charged. Due to the high H^+ concentration in the solution, there was a competitive adsorption of $HCrO_4^-$ with the Cr(VI) ions, thus decreasing the Cr(VI) removal efficiency (Chen et al., 2010). When the pH value was in the range of 3.3–6.0, the Cr(VI) removal efficiency decreased rapidly. The isoelectric point of diatomite is 5, giving rise to a positive surface charge in acidic solution. The Cr(VI) removal efficiency rapidly increased at pH = 8, possibly due to the combined effect of both chemical and electrostatic interactions between MnO_2 and diatomite. At higher pH values, however, the OH^- ions became the dominant species, resulting in a weakening of the electrostatic forces between the adsorbent and adsorbate, and hence leading to a reduced Cr(VI) removal efficiency (Xu et al., 2011; Chen et al., 2010). The Cr(VI) removal efficiency increased in the order diatomite < sheet-like MnO_2/diatomite < flower-like MnO_2/diatomite < wire-like MnO_2/diatomite. The fact that the Cr(VI) adsorption performance of the wire-like MnO_2/diatomite sample was best might be due to it having the largest surface area and more exposed active (310) and (211) crystal planes.

2.3.2. Influence of adsorption time on the adsorption of Cr(VI)

Fig. 6 shows the effect of adsorption time on the removal efficiency of the diatomite and MnO_2/diatomite samples under the conditions of Cr(VI) solution volume = 100 mL, initial Cr(VI) concentration = 50 mg/L, adsorbent mass = 0.04 g, pH = 2, and adsorption temperature = room temperature. From Fig. 6, one can see that the Cr(VI) removal efficiency increased with the extension of adsorption time, and reached a saturated value. The removal efficiency increased rapidly in the first 12 min and reached stability within 15 min. Therefore, the appropriate adsorption time was 30 min. The Cr(VI) removal efficiency of the MnO_2/diatomite samples was much higher than that of the diatomite sample, and the highest Cr(VI) removal efficiency (100% at an adsorption time of 30 min) was achieved over the wire-like MnO_2/diatomite sample. The rapid adsorption of Cr(VI) by the MnO_2/diatomite samples might be attributed to the external surface adsorption (Hu et al., 2005), during which the adsorbate had an easy access to the active adsorption sites of the diatomite-coated MnO_2 nanoparticles. The saturated Cr(VI) adsorption capacity increased in the

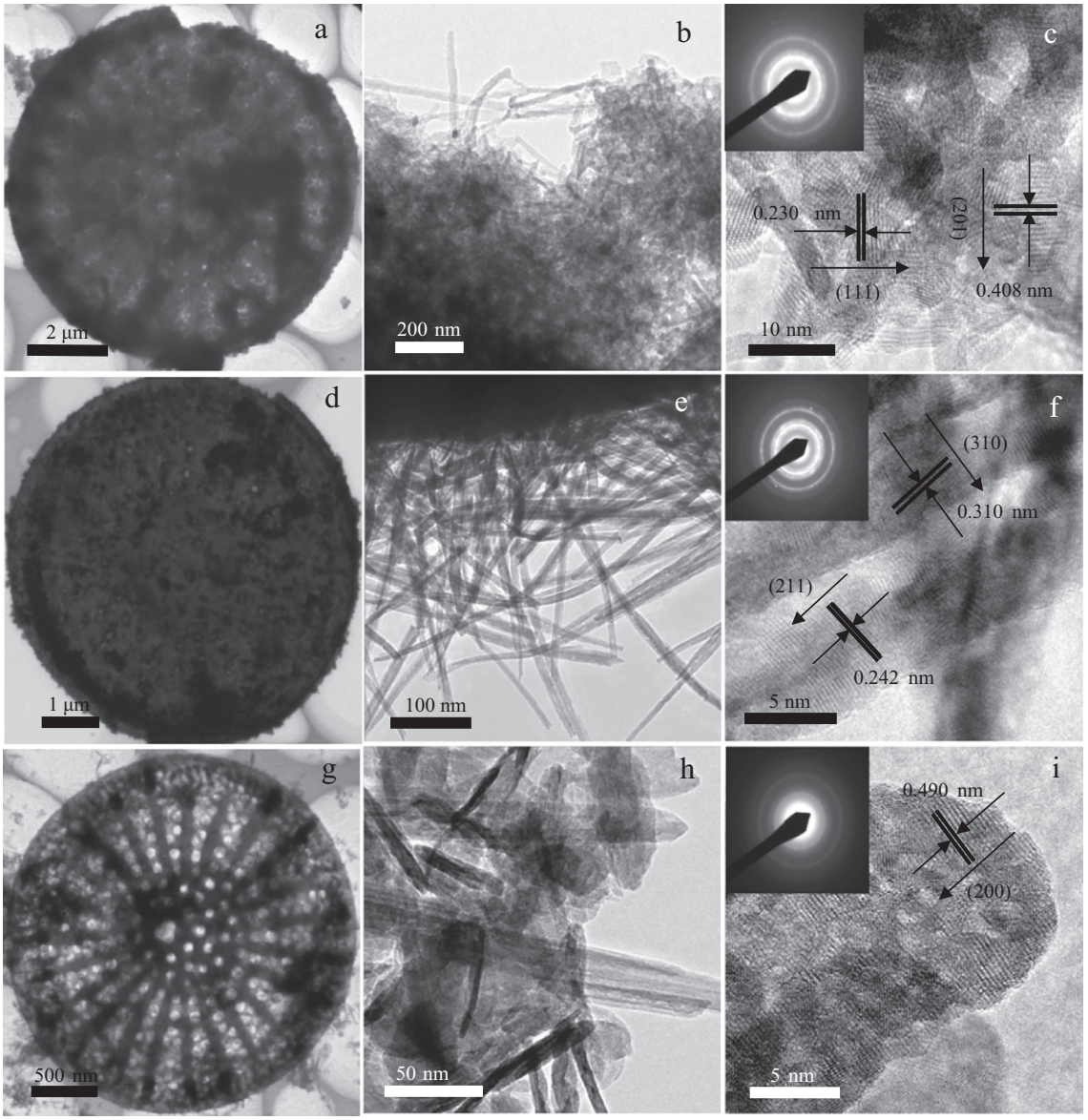

Fig. 3 – TEM images of (a–c) flower-like MnO_2/diatomite, (d–f) wire-like MnO_2/diatomite, and (g–i) sheet-like MnO_2/diatomite.

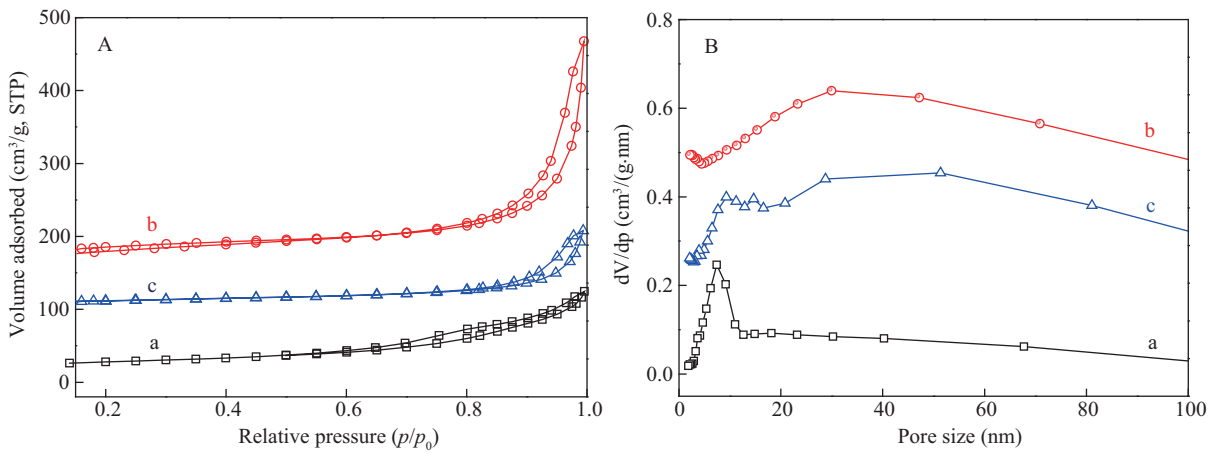

Fig. 4 – (A) N_2 adsorption-desorption isotherms and (B) pore-size distributions of (line a) flower-like MnO_2/diatomite, (line b) wire-like MnO_2/diatomite and (line c) sheet-like MnO_2/diatomite.

Table 1 – Preparation conditions and textural parameters of the MnO_2/diatomite samples.

Adsorbent	Preparation method	Mn source	BET surface area (m^2/g)	Average pore size (nm)
Diatomite	–	–	25.0	16.3
Flower-like MnO_2/diatomite	Hydrothermal treatment at 80°C for 4 hr	$Mn(Ac)_2$ and $KMnO_4$	66.5	10.7
Wire-like MnO_2/diatomite	Hydrothermal treatment at 90°C for 12 hr	$KMnO_4$	144.2	13.8
Sheet-like MnO_2/diatomite	Hydrothermal treatment at room temperature for 10 hr	$MnSO_4{\cdot}4H_2O$	49.5	14.2

C_0 (mg/L).

order of diatomite < sheet-like MnO_2/diatomite < flower-like MnO_2/diatomite < wire-like MnO_2/diatomite.

2.3.3. Influence of initial Cr(VI) concentration on the Cr(VI) adsorption behavior

Fig. 7 shows the effect of initial Cr(VI) concentration on the adsorption capacity of the diatomite and MnO_2/diatomite samples under the conditions of Cr(VI) solution volume = 50 mL, adsorbent mass = 0.04 g, pH = 2, adsorption time = 30 min, initial Cr(VI) concentration = 25, 50, 75, 100, 125, 150, 175, 200, 225 or 250 mg/L, and adsorption temperature = room temperature, and the calculated C_e, Q_e, and E values for the samples are summarized in Table 2. It was observed that the adsorption capacity increased with the rise in initial Cr(VI) concentration. This might be due to the availability of more Cr(VI) ions in the solution for adsorption on the surface active sites of the samples (Yang et al., 2013; Lo et al., 2006). The Cr(VI) adsorption capacities of the MnO_2/diatomite samples were much higher than that of the diatomite sample, with the highest Cr(VI) adsorption capacity (101 mg/g at a Cr(VI) concentration of 250 mg/L) being achieved over the wire-like MnO_2/diatomite sample (Table 2). At the same initial Cr(VI) concentration, the Cr(VI) adsorption capacity increased in the order diatomite < sheet-like MnO_2/diatomite < flower-like MnO_2/diatomite < wire-like MnO_2/diatomite. Usually, the Cr(VI) concentrations of most wastewater are in the range of 10–150 mg/L. According to the United States Environmental Protection Agency (USEPA), the maximal permissible Cr(VI) limit is 0.1 mg/L for discharging into inland surface water and 0.05 mg/L for potable water. Under the adopted conditions, when the initial Cr(VI) concentration was below 25 mg/L, the removal efficiency was maintained above 96% (C_e = 0.02 mg/L) over the wire-like MnO_2/diatomite sample, which meets the USEPA standard for the drinking water; the C_e value achieved over the flower-like MnO_2/diatomite sample was 0.1 mg/L, which meets the USEPA standard for industrial wastewater; with the rise in initial Cr(VI) concentration from 25 to 250 mg/L, however, the removal efficiency decreased. Table 3 summarizes the Cr(VI) removal efficiency and adsorption capacities of our samples and different adsorbents reported in the literature. Clearly, the Cr(VI) removal efficiency over our wire-like MnO_2/diatomite sample was much higher than those over the EDA-PSt (Cui et al., 2013) and ADAS-based activated carbon (Gorzin and Ghoreyshi, 2013) samples, and slightly higher than Ca–Al LDHs (Li et al., 2013a,b), TAC/Fe (Liu et al., 2012), *Eichhornia crassipes* root biomass-derived activated carbon (Giri et al., 2012), dodecylamine-modified sodium montmorillonite (Kumar et al., 2012), and HDTMA-modified natural red clay (Gładysz-Płaska et al., 2012) samples. Since the Cr(VI) removal efficiency is associated with the Cr(VI) concentration and adsorbent mass,

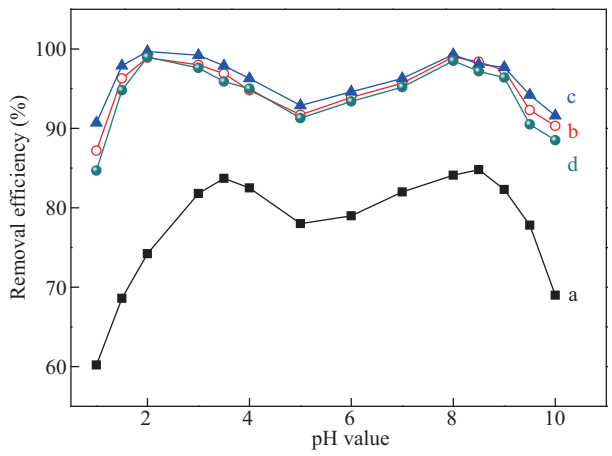

Fig. 5 – Effect of pH value on the Cr(VI) removal efficiency of (line a) diatomite, (lien b) flower-like MnO_2/diatomite, (line c) wire-like MnO_2/diatomite, and (line d) sheet-like MnO_2/diatomite.

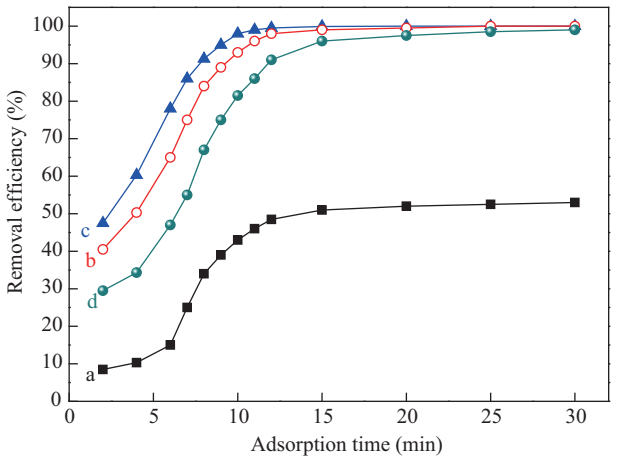

Fig. 6 – Effect of adsorption time on the Cr(VI) removal efficiency of (line a) diatomite, (line b) flower-like MnO_2/diatomite, (line c) wire-like MnO_2/diatomite, and (line e) sheet-like MnO_2/diatomite.

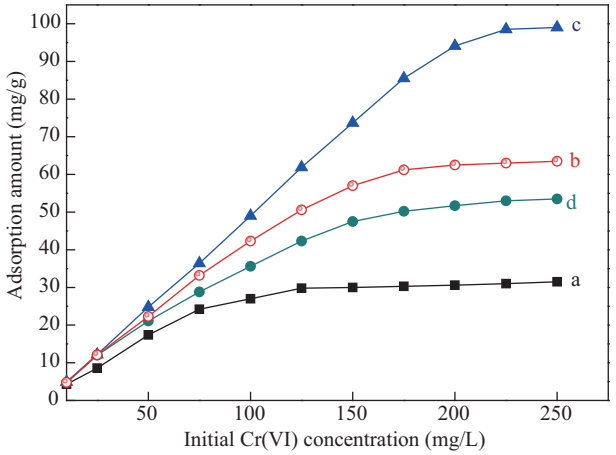

Fig. 7 – Effect of initial Cr(VI) concentration on the Cr(VI) adsorption amount of (line a) diatomite, (line b) flower-like MnO_2/diatomite, (line c) wire-like MnO_2/diatomite, and (line d) sheet-like MnO_2/diatomite.

the appropriate parameter for evaluating the Cr(VI) adsorption behavior of an adsorbent is the Cr(VI) adsorption capacity. It is observed from Table 3 that the Cr(VI) adsorption capacities of the MnO_2/diatomite samples obtained in the present work were comparable with those of the Ca–Al LDH sample (Li et al., 2013a,b), and higher than those of ADAS-based activated carbon (Gorzin and Ghoreyshi, 2013) and the other nonmetallic mineral adsorbents. Although the EDA-PSt (Cui et al., 2013) and PA6@Fe_xO_y (Li et al., 2013a,b) samples showed better Cr(VI) adsorption performance than our samples, the former are much more expensive (limiting their engineering applications). In addition, the cheaper natural adsorbents (*e.g.*, clay, TA-AC, montmorillonite, and so on (Kumar et al., 2012; Wen et al., 2011; Li et al., 2012; Thanos et al., 2012)) did not possess high Cr(VI) adsorption capacities. Therefore, our inexpensive MnO_2/diatomite samples are promising for practical applications in the removal of Cr(VI) from industrial wastewater.

2.3.4. Adsorption stability of the samples

Fig. 8 shows the Cr(VI) adsorption capacity *versus* the number of Cr(VI) adsorption/desorption cycles on the diatomite, flower-like MnO_2/diatomite, wire-like MnO_2/diatomite, and sheet-like MnO_2/diatomite samples. It can be seen that after 8 cycles of Cr(VI) adsorption/desorption, the maximal Cr(VI) adsorption capacities of the diatomite, flower-like MnO_2/diatomite, wire-like MnO_2/diatomite, and sheet-like MnO_2/diatomite samples decreased by 18.4%, 27.6%, 18.3%, and 26.4%, respectively. Clearly, the diatomite and wire-like MnO_2/diatomite samples showed better Cr(VI) adsorption stability than the flower-like MnO_2/diatomite and sheet-like MnO_2/diatomite samples. Because the Cr(VI) adsorption capacity of wire-like MnO_2/diatomite was much larger than that of diatomite, the former was far superior to the latter in adsorbing Cr(VI).

2.4. Cr(VI) adsorption mechanism

To confirm the above-mentioned deduction, we recorded the FT-IR spectra of the wire-like MnO_2/diatomite samples before and after the adsorption of Cr(VI) at pH = 2; at the same time we also recorded the FT-IR spectra of the raw diatomite samples before and after the deposition of wire-like MnO_2, as shown in Fig. 9. It is seen that the absorption peaks centered at 3450 and 1637 cm^{-1} were due to the stretching and bending vibrations of the –OH group in diatomite (Fig. 9a–c). The presence of SiO_2 was verified by the detection of absorption peaks centered at 1100 and 465 cm^{-1}, which were due to the asymmetrical stretching and bending vibrations of the Si–O–Si bond in diatomite, respectively. The absorption peak centered at 798 cm^{-1} was attributable to the Si–O–Al bond (Huang et al., 2007). The wire-like MnO_2/diatomite sample showed six absorption peaks centered at 528, 622, 1110, 1400, 1637, and 3186 cm^{-1}: The peaks at 528 and 622 cm^{-1} could be ascribed to the Mn–O bending vibrations (Tang et al., 2010), those at 1637, 1400, and 1110 cm^{-1} were attributed to the bending vibrations of –OH group attached to the Mn atoms (Yuan et al., 2010a,b), and the broad one at 3186 cm^{-1} could be assigned to the stretching vibration of the –OH group in adsorbed water (Li et al., 2007). After the adsorption of Cr(VI), new absorption peaks centered at 581 and 860 cm^{-1} appeared, ascribable to the stretching vibrations of the Cr–O or Cr–O–Cr bond (Lakshmipathiraj et al., 2013). The new absorption peak at 2071 cm^{-1} corresponded to the stretching vibration of the Cr═O bond, which suggests that the Cr(VI) species had interacted with the surface hydroxyl groups of the sample.

Table 2 – Cr(VI) removal efficiency (*E*) of the MnO_2/diatomite samples at different initial Cr(VI) concentrations (C_0).

Sample	C_0 (mg/L)	10	25	50	75	100	125	150	175	200	225	250
Wire-like MnO_2/diatomite	C_e (mg/L)	0.02	1.0	7.8	17.4	28.8	40.4	55.0	74.6	96.6	119.0	143.0
	Q_e (mg/g)	4.99	12.0	21.1	28.8	35.6	42.3	47.5	50.2	51.7	53.0	53.5
	E (%)	99.8	96.0	84.4	76.8	71.2	67.7	63.3	57.4	51.7	47.1	42.8
Flower-like MnO_2/diatomite	C_e (mg/L)	0.1	0.6	0.4	2.2	2.0	1.2	2.6	4.0	11.8	28.0	52.0
	Q_e (mg/g)	4.95	12.2	24.8	36.4	49.0	61.9	73.7	85.5	94.1	98.5	99.0
	E (%)	99.0	97.6	99.2	97.1	98.0	99.0	98.3	97.7	94.1	87.6	79.2
Sheet-like MnO_2/diatomite	C_e (mg/L)	0.4	0.8	5.4	8.6	15.4	23.8	36.0	52.6	75.0	99.0	123.0
	Q_e (mg/g)	4.8	12.1	22.3	33.2	42.3	50.6	57.0	61.2	62.5	63.0	63.5
	E (%)	96.0	96.8	89.2	88.5	84.6	80.9	76.0	69.9	62.5	56.0	50.8

Adsorption conditions: Cr(VI) solution volume = 50 mL, adsorbent mass = 0.04 g, pH = 2, adsorption time = 30 min, and adsorption temperature = room temperature.

Table 3 – Cr(VI) removal efficiency and adsorption capacities of various adsorbents.

Adsorbent	Optimal pH value	Removal efficiency (%)	Adsorption capacity (mg/g)	Reference
Flower-like MnO_2/diatomite	2 or 8	99.0	61.2	This work
Wire-like MnO_2/diatomite	2 or 8	99.98	101.4	This work
Sheet-like MnO_2/diatomite	2 or 8	96.0	48.2	This work
EDA-PSt	2	77.3	175.8	Cui et al. (2013)
ADAS-based activated carbon	2	78.0	70.2	Gorzin and Ghoreyshi (2013)
Ca–Al hydrotalcite (Ca–Al LDHs)	11	98.8	104.8	Li et al. (2013a, 2013b)
TAC	2	93.9	49.0	Liu et al. (2012)
TAC/Fe	2	99.6	68.5	Liu et al. (2012)
Eichhornia crassipes root biomass-derived activated carbon	4.5	92.2	36.3	Giri et al. (2012)
Dodecylamine-modified sodium montmorillonite	–	99.6	23.7	Kumar et al. (2012)
HDTMA-modified natural red clay	5.5	97.0	0.1	Gładysz-Płaska et al. (2012)
PA6@Fe_xO_y	–	–	175.8	Li et al. (2013a, 2013b)
Chitosan-coated fly ash	5.5	–	33.3	Wen et al. (2011)
TA-AC (tannin-immobilized activated clay)	2.5	–	24.1	Li et al. (2012)
Zeolite	4	–	13.2	46
Vermiculite	4	–	27.1	46
Bentonite	4	–	24.2	46
Attapulgite	4	–	15.3	46

The shifts in absorption peaks from 1100 to 1137 cm^{-1} and from 1400 to 1439 cm^{-1} were possibly due to the interaction of Si–O–Si and carboxylic groups with Cr(VI), respectively. Another shift was observed from 1637 to 1537 cm^{-1}, corresponding to the complexation of hydroxyl groups with Cr(VI). The results indicate that the structure of the wire-like MnO_2/diatomite sample was not significantly changed after Cr(VI) adsorption; for the wire-like MnO_2/diatomite sample, the Mn–O bonds, hydroxyl groups attached to the Mn atoms, and carboxyl groups may play a major role in the adsorption of Cr(VI).

Fig. 10a and b shows the full-scan XPS spectra of the wire-like MnO_2/diatomite samples before and after the adsorption of Cr(VI) at pH = 2. It can be seen that Si, Mn, Cr, O, and C were present on the surface of the wire-like MnO_2/diatomite sample; furthermore, two well-resolved Cr 2p XPS peaks at BE = 579.5 and 588.7 eV (attributable to the Cr $2p_{3/2}$ and Cr $2p_{1/2}$ final states (Cao et al., 2012), respectively) were observed as shown in Fig. 10b. This result indicates the occurrence of Cr(VI) adsorption. From Fig. 10c, one can observe three O 1s XPS peaks at BE = 529.8, 531.1, and 532.6 eV, assignable to the surface lattice oxygen species on MnO_2, surface lattice oxygen species on diatomite, and adsorbed hydroxyl species on diatomite, respectively. After Cr(VI) adsorption over the wire-like MnO_2/diatomite sample (Fig. 10d), three O 1s XPS peaks at BE = 529.8, 531.3, and 532.8 eV were observed, which could be attributed to the surface lattice oxygen species on MnO_2 and adsorbed Cr(VI) like CrO_3 (Fig. 10c), surface lattice oxygen species on diatomite, and physically adsorbed water species on diatomite, respectively. Clearly, the surface –OH concentration of wire-like MnO_2/diatomite before Cr(VI) adsorption was higher than that after Cr(VI) adsorption, indicating that the hydroxyl

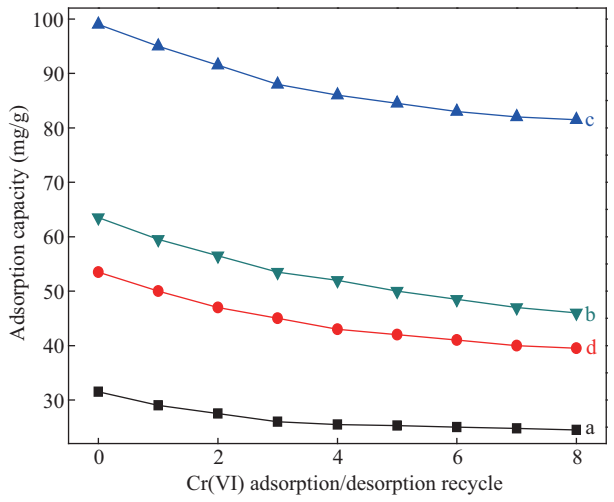

Fig. 8 – Cr(VI) adsorption capacity *versus* the number of Cr(VI) adsorption/desorption recycle on (line a) diatomite, (line b) flower-like MnO_2/diatomite, (line c) wire-like MnO_2/diatomite, and (line d) sheet-like MnO_2/diatomite.

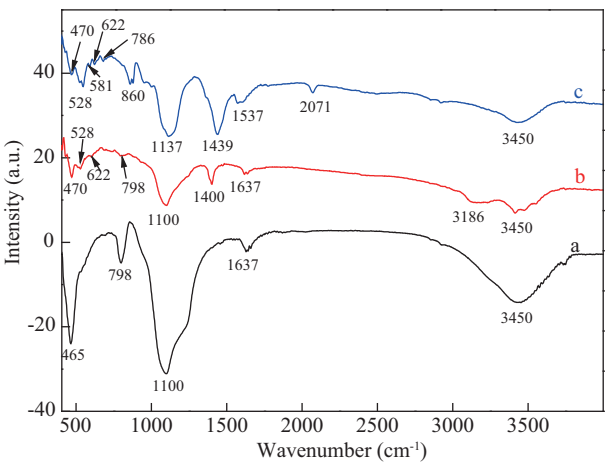

Fig. 9 – FT-IR spectra of (line a) raw diatomite and wire-like MnO_2/diatomite (line b) before and (line c) after Cr(VI) adsorption.

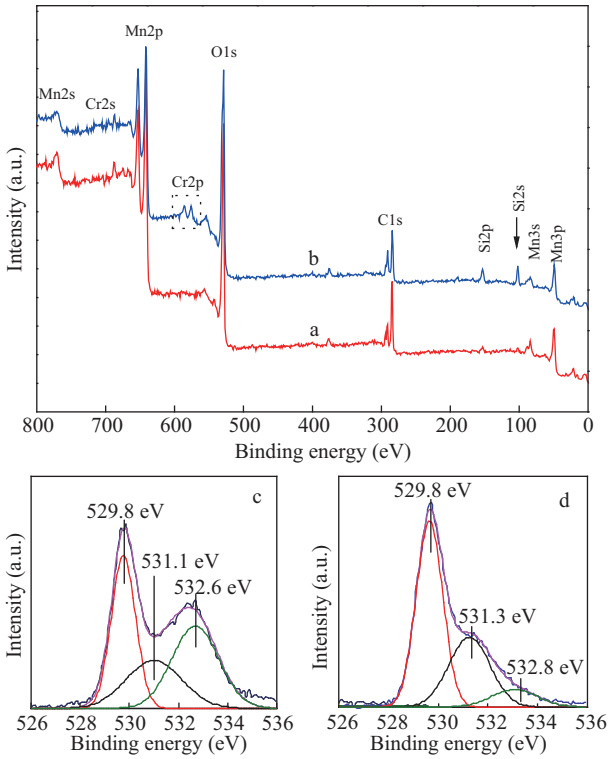

Fig. 10 – (a) Full-scan XPS spectrum of wire-like MnO_2/diatomite before and after Cr(VI) adsorption, (b) O 1s XPS spectrum of wire-like MnO_2/diatomite, and (c) O 1s spectrum of wire-like MnO_2/diatomite after Cr(VI) adsorption.

groups had been exchanged with $Cr_2O_7^{2-}$ or $HCrO_4^-$ in the Cr(VI) solutions. Therefore, hydroxyl groups played a critical role in Cr(VI) adsorption.

The Langmuir and Freundlich isotherm models are most commonly used in effectively describing adsorption modes. The former assumes the monolayer adsorption of metal ions on a homogenous surface, whereas the latter describes multilayer adsorption of metal ions on a heterogeneous surface. The Langmuir and Freundlich isotherm equations can be expressed as follows:

$$\text{Langmuir isotherm equation}: \quad 1/Q_e = 1/(Q_0 \times C_e \times K_L) + 1/Q_0$$

$$\text{Freundlich isotherm equation}: \quad \log Q_e = 1/n \ \log C_e + \log K_F$$

where, C_e (mg/L), Q_e (mg/g), Q_0 (mg/g), K_L, n, and K_F are the equilibrium concentration, equilibrium adsorption capacity, maximal adsorption capacity, Langmuir constant, and Freundlich constants, respectively.

Table 4 summarizes the main adsorption isotherm parameters. It can be seen that the adsorption data obtained over the MnO_2/diatomite samples were more consistent with the Langmuir isotherm model than the Freundlich isotherm model, whereas the diatomite sample was more fit better by the Freundlich isotherm model than the Langmuir isotherm model. Furthermore, the adsorption of Cr(VI) on the surface of the MnO_2/diatomite samples was favorable due to the $1/n$ value range of 0.1–1.0, and the adsorption capacity followed the sequence of wire-like/diatomite > flower-like MnO_2/diatomite > sheet-like MnO_2/diatomite > diatomite. The different adsorption capacities of these samples might result from the various structures and functional groups as well as their surface distributions.

3. Conclusions

By using a hydrothermal method, we generated flower-, wire-, and sheet-like MnO_2-coated diatomite adsorbents with high surface areas (49.5–144.2 m^2/g). The adsorption of Cr(VI) was greatly influenced by the pH of the Cr(VI) aqueous solution. The highest Cr(VI) removal efficiency (96.0%–99.98% at initial Cr(VI) concentration of 10 mg/L and pH 2.0 or 8.0) was observed over the MnO_2-coated diatomite samples with different morphologies, and the maximal Cr(VI) adsorption capacity reached 101 mg/g over the wire-like MnO_2/diatomite sample. The kinetic data reveals that the Cr(VI) adsorption over the MnO_2/diatomite samples was fit better by the Langmuir model.

Acknowledgments

This work described above was financially supported by the Science and Technology Program of Jilin Province (Nos. 20130305015GX, 2014204037SF), and the Beijing Natural Science Foundation (No. 2142008), and the National Natural Science Foundation of China (No. 51225402).

Appendix A. Supplementary data

Supplementary data to this article can be found online at http://dx.doi.org/10.1016/j.jes.2014.06.047.

Table 4 – Langmuir and Freundlich equations for the adsorption of Cr(VI) on the diatomite and MnO_2/diatomite samples.

Adsorbent	Langmuir equation			Freundlich equation		
	K_L	Q_0 (mg/g)	R^2	$\log K_F$	$1/n$	R^2
Diatomite	0.1329	29.4	0.9537	0.6151	0.3411	0.9773
Flower-like MnO_2/diatomite	0.2289	61.2	0.9861	1.040	0.3415	0.9307
Wire-like MnO_2/diatomite	0.0869	101.4	0.9938	1.1498	0.3572	0.9321
Sheet-like MnO_2/diatomite	0.3301	48.2	0.9889	0.9877	0.3518	0.9385

REFERENCES

Ajmal, M., Rao, R.A.K., Siddiqui, B.A., 1996. Studies on removal and recovery of Cr(VI) from electroplating water. Water Res. 30, 1478–1482.

Ajouyed, O., Hurel, C., Ammari, M., Allal, L.B., Marmier, N., 2010. Marmier. Sorption of Cr(VI) onto natural iron and aluminum(oxy) hydroxides: effects of pH, ionic strength and initial concentration. J. Hazard. Mater. 174, 616–622.

Al-Degs, Y.S., Khraisheh, M.A.M., Tutunji, M.F., 2001. Sorption of lead ions on diatomite and manganese oxides modified diatomite. Water Res. 35, 3724–3728.

Al-Ghouti, M.A., Al-Degs, Y.S., 2011. New adsorbents based on microemulsion modified diatomite and activated carbon for removing organic and inorganic pollutants from waste lubricants. Chem. Eng. J. 173, 115–128.

Al-Ghouti, M.A., Khraishehb, M.A.M., Tutuji, M., 2004. Flow injection potentiometric stripping analysis for study of adsorption of heavy metal ions onto modified diatomite. Chem. Eng. J. 104, 83–91.

Almeida, M.A.F., Boaventura, R.A.R., 1997. Chromium precipitation from tanning spent liquors using industrial alkaline residues: a comparative study. Waste Manag. 17, 201–209.

Cao, C.Y., Qu, J., Yan, W.S., Zhu, J.F., Wu, Z.Y., 2012. Low-cost synthesis of flowerlike α-Fe_2O_3 nanostructures for heavy metal ion removal: adsorption property and mechanism. Langmuir 28, 4573–4579.

Chen, S.H., Yue, Q.Y., Gao, B.Y., Xu, X., 2010. Equilibrium and kinetic adsorption study of the adsorptive removal of Cr(VI) using modified wheat residue. J. Colloid Interface Sci. 349, 256–264.

Choi, H.-D., Jung, W.-S., Cho, J.-M., Ryu, B.-G., Yang, J.-S., 2009. Adsorption of Cr(VI) onto cationic surfactant-modified activated carbon. J. Hazard. Mater. 166, 642–646.

Cui, L.L., Meng, Q.Q., Zheng, J.Y., Wei, X., Ye, Z.F., 2013. Adsorption of Cr(VI) on 1,2-ethylenediamine-aminated macroporous polystyrene particles. Vacuum 89, 1–6.

Danil de Namor, A.F., Gamouz, A.E., Frangie, S., Martinez, V., 2012. Turning the volume down on heavy metals using tuned diatomite. A review of diatomite and modified diatomite for the extraction of heavy metals from water. J. Hazard. Mater. 241–242, 14–31.

Farag, A.M., May, T., Marty, G.D., Easton, M., Harper, D.D., 2006. The effect of chronic chromium exposure on the health of Chinook salmon (*Oncorhynchus tshawytscha*). Aquat. Toxicol. 76, 246–257.

Giri, A.K., Patel, R., Mandal, S., 2012. Removal of Cr(VI) from aqueous solution by *Eichhornia crassipes* root biomass-derived activated carbon. Chem. Eng. J. 185–186, 71–81.

Gładysz-Płaska, A., Majdan, M., Pikus, S., Sternik, D., 2012. Simultaneous adsorption of chromium(VI) and phenol on natural red clay modified by HDTMA. Chem. Eng. J. 179, 140–150.

Gorzin, F., Ghoreyshi, A.A., 2013. Synthesis of a new low-cost activated carbon from activated sludge for the removal of Cr(VI) from aqueous solution: equilibrium, kinetics, thermodynamics and desorption studies. Korean J. Chem. Eng. 30, 1594–1602.

Gülay, B., Mehmet, Y.A., 2008. Adsorption of Cr(VI) onto PEI immobilized acrylate-based magnetic beads: isotherms, kinetics and thermodynamics study. Chem. Eng. J. 139, 20–28.

Gupta, S., Babu, B.V., 2009. Utilization of waste product (tamarind seeds) for the removal of Cr(VI) from aqueous solutions: equilibrium, kinetics, and regeneration studies. J. Environ. Manag. 90, 3013–3022.

Gzara, L., Dhahbi, M., 2001. Removal of chromate anions by micellar-enhanced ultrafiltration using cationic surfactants. Desalination 137, 241–250.

Han, X., Wong, Y.S., Wong, M.H., Tam, N.F.Y., 2008. Effects of anion species and concentration on the removal of Cr(VI) by amicroalgal isolate, *Chlorella miniata*. J. Hazard. Mater. 158, 615–620.

Hu, J., Chen, G.H., Lo, I.M.C., 2005. Removal and recovery of Cr(VI) from waste water by maghemite nanoparticles. Water Res. 39, 4528–4536.

Huang, J.H., Liu, Y.F., Jin, Q.Z., Wang, X.G., Yang, J., 2007. Adsorption studies of a water soluble dye, reactive red MF-3B, using sonication-surfactant-modified attapulgite clay. J. Hazard. Mater. 143, 541–548.

Julien, C., Massot, M., 2002. Spectroscopic studies of the local structure in positive electrodes for lithium batteries. Phys. Chem. Chem. Phys. 4, 4226–4235.

Khraisheh, M.A.M., Al-Degs, Y.S., Mcminn, W.A.M., 2004. Remediation of wastewater containing heavy metals using raw and modified diatomite. Chem. Eng. J. 99, 177–184.

Kozlowski, C.A., Walkowiak, W., 2002. Removal of chromium(VI) from aqueous solutions by polymer inclusion membranes. Water Res. 36, 4870–4876.

Kumar, A.S.K., Ramachandran, R., Kalidhasan, S., Rajesh, V., Rajesh, N., 2012. Potential application of dodecylamine modified sodium montmorillonite as an effective adsorbent for hexavalent chromium. Chem. Eng. J. 211–212, 396–405.

Lakshmipathiraj, P., Umamaheswari, S., Raju, G.B., Prabhakar, S., Caroling, G., 2013. Adsorption of Cr(VI) onto *Strychnos potatorum* seed from aqueous solution. Environ. Prog. Sustain. Energy 32, 35–41.

Li, L.P., Pan, Y.Z., Chen, L.J., Li, G.S., 2007. One-dimensional α-MnO_2: trapping chemistry of tunnel structures, structural stability, and magnetic transitions. Solid State Chem. 180, 2896–2904.

Li, E., Zeng, X.Y., Fan, Y.H., 2009. Removal of chromium ion (III) from aqueous solution by manganese oxide and microemulsion modified diatomite. Desalination 238, 158–165.

Li, W., Tang, Y.K., Zeng, Y.T., Tong, Z.F., Liang, D.W., 2012. Adsorption behavior of Cr(VI) ions on tannin-immobilized activated clay. Chem. Eng. J. 193–194, 88–95.

Li, Y.L., Wang, J., Li, Z.S., Liu, Q., Liu, J.Y., Liu, L.H., Zhang, X.F., Yu, J., 2013a. Ultrasound assisted synthesis of Ca–Al hydrotalcite for U(VI) and Cr(VI) adsorption. Chem. Eng. Water Res. J. 218, 295–302.

Li, C.J., Li, Y.J., Wang, J.N., Cheng, J., 2013b. PA6@Fe_xO_y nanofibrous membrane preparation and its strong Cr(VI)-removal performance. Chem. Eng. J. 220, 294–301.

Liu, W.F., Zhang, J., Zhang, C.L., Ren, L., 2012. Preparation and evaluation of activated carbon-based iron-containing adsorbents for enhanced Cr(VI) removal: mechanism study. Chem. Eng. J. 189–190, 295–302.

Lo, I.M.C., Lam, C.S.C., Lai, K.C.K., 2006. Hardness and carbonate effects on the reactivity of zero-valent iron for Cr(VI) removal. Water Res. 40, 595–605.

Martell, A.E., Hancock, R.D., 1996. Metal Complexes in Aqueous Solutions. Plenum Press, New York.

Metin, G., Duygu, V., Ayse, M., 2008. Removal of trivalent chromium from water using low-cost natural diatomite. J. Hazard. Mater. 160, 318–323.

Mohanty, K., Jha, M., Meikap, B.C., Biswas, M.N., 2005. Removal of chromium(VI) from dilute aqueous solutions by activated carbon developed from *Terminalia arjuna*. Chem. Eng. Sci. 60, 3049–3059.

Mohanty, K., Jha, M., Meikap, B.C., Biswas, M.N., 2006. Biosorption of Cr(VI) from aqueous solutions by *Eichhornia crassipes*. Chem. Eng. J. 117, 71–77.

Muradiye, U., Irfan, A., 2007. Removal of Cr(VI) from industrial wastewaters by adsorption part I: determination of optimum conditions. J. Hazard. Mater. 149, 482–491.

Pagana, A.E., Sklari, S.D., Kikkinides, E.S., Zaspalis, V.T., 2011. Combined adsorption–permeation membrane process for the

removal of chromium(III) ions from contaminated water. J. Membr. Sci. 367, 319–324.
Sheng, G.D., Wang, S.W., Hu, J., Lu, Y., Li, J.X., 2009. Adsorption of Pb(II) on diatomite as affected via aqueous solution chemistry and temperature. Colloids Surf. A 339, 159–166.
Sungworawongpana, S., Pengprecha, S., 2011. Calcination effect of diatomite to chromate adsorption. Procedia Eng. 8, 53–57.
Taha, A.A., Wu, Y.N., Wang, H.T., Li, F.T., 2012. Preparation and application of functionalized cellulose acetate/silica composite nanofibrous membrane via electrospinning for Cr(VI) ion removal from aqueous solution. J. Environ. Manag. 112, 10–16.
Tang, N., Tian, X.K., Yang, C., Pi, Z.B., Han, Q., 2010. Facile synthesis of α-MnO_2 nanorods for high-performance alkaline batteries. J. Phys. Chem. Solids 71, 258–262.
Thanos, A.G., Katsou, E., Malamis, S., Psarras, K., Pavlatou, E.A., 2012. Evaluation of modified mineral performance for chromate sorption from aqueous solutions. Chem. Eng. J. 211–212, 77–88.
Wen, Y., Tang, Z.R., Chen, Y., Gu, Y.X., 2011. Adsorption of Cr(VI) from aqueous solutions using chitosan-coated fly ash composite as biosorbent. Chem. Eng. J. 175, 110–116.
Williford Jr., C.W., Bricka, R.M., Foster, C.C., 2002. Reduction of suspended solids following hydroclassification of metal-contaminated soils. J. Hazard. Mater. 92, 63–75.
Xu, X., Gao, B.Y., Tan, X., Yue, Q.Y., Zhong, Q.Q., 2011. Characteristics of amine-crosslinked wheat straw and its adsorption mechanisms for phosphate and chromium(VI) removal from aqueous solution. Carbohydr. Polym. 84, 1054–1060.
Yang, X.L., Wang, X.Y., Feng, Y.Q., Zhang, G.Q., Wang, T.S., 2013. Removal of multifold heavy metal contaminations in drinking water by porous magnetic Fe_2O_3@AlO(OH) super structure. J. Mater. Chem. A 1, 473–477.
Yuan, A.B., Wang, X.L., Wang, Y.Q., Hu, J., 2010a. Comparison of nano-MnO_2 derived from different manganese sources and influence of active material weight ratio on performance of nano-MnO_2/activated carbon supercapacitor. Energy Convers. Manag. 51, 2588–2594.
Yuan, P., Liu, D., Fan, M.D., Yang, D., Zhu, R.L., 2010b. Removal of hexavalent chromium [Cr(VI)] from aqueous solutions by the diatomite-supported/unsupported magnetite nanoparticles. J. Hazard. Mater. 173, 614–621.
Zhuravlev, L.T., 2000. The surface chemistry of amorphous silica. Zhuravlev model. Colloids Surf. A 173, 1–38.

Editorial Board of Journal of Environmental Sciences

JOURNAL OF ENVIRONMENTAL SCIENCES

环境科学学报(英文版)

www.jesc.ac.cn

Aims and scope

Journal of Environmental Sciences is an international academic journal supervised by Research Center for Eco-Environmental Sciences, Chinese Academy of Sciences. The journal publishes original, peer-reviewed innovative research and valuable findings in environmental sciences. The types of articles published are research article, critical review, rapid communications, and special issues.

The scope of the journal embraces the treatment processes for natural groundwater, municipal, agricultural and industrial water and wastewaters; physical and chemical methods for limitation of pollutants emission into the atmospheric environment; chemical and biological and phytoremediation of contaminated soil; fate and transport of pollutants in environments; toxicological effects of terrorist chemical release on the natural environment and human health; development of environmental catalysts and materials.

For subscription to electronic edition

Elsevier is responsible for subscription of the journal. Please subscribe to the journal via http://www.elsevier.com/locate/jes.

For subscription to print edition

China: Please contact the customer service, Science Press, 16 Donghuangchenggen North Street, Beijing 100717, China. Tel: +86-10-64017032; E-mail: journal@mail.sciencep.com, or the local post office throughout China (domestic postcode: 2-580).

Outside China: Please order the journal from the Elsevier Customer Service Department at the Regional Sales Office nearest you.

Submission declaration

Submission of the work described has not been published previously (except in the form of an abstract or as part of a published lecture or academic thesis), that it is not under consideration for publication elsewhere. The publication should be approved by all authors and tacitly or explicitly by the responsible authorities where the work was carried out. If the manuscript accepted, it will not be published elsewhere in the same form, in English or in any other language, including electronically without the written consent of the copyright-holder.

Editorial

Authors should submit manuscript online at http://www.jesc.ac.cn. In case of queries, please contact editorial office, Tel: +86-10-62920553, E-mail: jesc@rcees.ac.cn. Instruction to authors is available at http://www.jesc.ac.cn.

Journal of Environmental Sciences (Established in 1989)
Volume 29 2015

Supervised by	Chinese Academy of Sciences	**Published by**	Science Press, Beijing, China
Sponsored by	Research Center for Eco-Environmental		Elsevier Limited, The Netherlands
	Sciences, Chinese Academy of Sciences	**Distributed by**	
Edited by	Editorial Office of Journal of	Domestic	Science Press, 16 Donghuangchenggen
	Environmental Sciences		North Street, Beijing 100717, China
	P. O. Box 2871, Beijing 100085, China		Local Post Offices through China
	Tel: 86-10-62920553; http://www.jesc.ac.cn	Foreign	Elsevier Limited
	E-mail: jesc@rcees.ac.cn		http://www.elsevier.com/locate/jes
Editor-in-chief	X. Chris Le	**Printed by**	Beijing Beilin Printing House, 100083, China

CN 11-2629/X **Domestic postcode: 2-580** **Domestic price per issue RMB ¥ 110.00**

ISSN 1001-0742